Investigation of the effective wear of enamel accounting for microstructure and phase properties

Y. Yang, D. Yang, Q.-C. He

Version of Record: https://www.sciencedirect.com/science/article/pii/S0043164818316946
Manuscript_5a37f26b733f8a8ad22d0b8f9193d62c

Investigation of the effective wear of enamel accounting for microstructure and phase properties

Y. Yang[a], D. Yang[a,*], Q.-C. He[a,b,*]

[a] *School of Mechanical Engineering, Tribology Research Institute, Southwest Jiaotong University, Chengdu 610031, China*
[b] *Université Paris-Est, Laboratoire Modélisation et Simulation Multi Echelle, MSME UMR 8208 CNRS, 5 bd Descartes, 77454 Marne-la-Vallée Cedex 2, France*

Abstract

The effective wear behavior of enamel is investigated by considering the microstructure of enamel and the wear properties of the rod and interrod phases forming it. This investigation is guided by a recently proposed micromechanics theory of wear and realized by using the finite element method. A representative surface element is determined for the unilateral frictional contact with wear between enamel and a ball assimilated to food. Accounting for the elastic properties and wear characteristics of the rod and interrod phase, using different friction coefficients and considering sliding directions, the effective (or overall) wear coefficient of enamel is quantitatively determined for different inclination angles of the rod phase. The results of the present work suggests the existence of an optimal inclination angle of the rod phase for reducing the effective wear of enamel, which can be inspiring for optimizing the fiber orientation for a better wear-resistant fiber-reinforced composites.

Keywords: Wear; Enamel; Microstructure; Finite element; Archard law

1. Introduction

Dental enamel in the human body is the hardest tissue and possesses remarkable wear resistance. Its mass consists of 96% mineral and 4% organic material and water [1, 2, 3]. The exquisite hierarchical microstructure of enamel contributes to its high hardness, toughness

*Corresponding author
Email addresses: yangdan1234-2004@163.com (D. Yang), qi-chang.he@u-pem.fr (Q.-C. He)

and anti-wear behavior. At the scale of "multi-rods" which is around 50 μm [3], the key-hole shaped rods are regularly distributed and separated by organic-riched interrod layer in the view of the occlusal direction (Fig. 1). The long axis of rod bundles is arranged vertically to the occlusal surface until a certain depth beneath the surfacial layer and turns into a curved pattern in the inner layer of enamel [4, 5]. The depth of layer with vertical rods approximately represents one third of the total depth of enamel while the curved layer takes up the rest two thirds [6]. The geometric features of the fibrous structure of enamel, in particular, the key-hole shape of rods and the orientation of rod bundles, vary with mammals having different eating habits [7, 8] and may significantly affect the fracture and wear property of enamel [9]. Meanwhile, enamel grinds food or hard objects over the service life of teeth and the variation of enamel microstructure result in different degrees of damage in the counterparts. It is important to understand how these geometric features relate to its macroscopic resistance to wear and the efficiency of breaking objects in contact with enamel.

A large group of studies focus on the mechanical property of enamel at different scales, in particularly, at the scale of one single rod to multiple rods. In the aspect of experiments, nanoindentation is a widely applied tool to characterize the mechanical properties, i.e. elastic modulus and hardness of rod and interrod phase. The rod phase exhibits significantly higher elastic modulus and hardness compared with the interrod phase [10, 11]. Due to a small amount of proteins, the constitutive law of enamel is time-dependent. The viscosity of enamel makes energy dissipated under dynamic loading condition [11, 12, 13]. There exists a discrepancy of the mechanical parameters in testing. Numerical simulations by finite element were proposed to characterize the effective elastic modulus of enamel [4]. The tribological behavior of enamel is also highly associated to the anisotropic microstructure [14]. The nano-scratch technique can record the friction coefficient in rod and interrod region and the depth of wear scar representing the wear resistance of rod or interrod phase. Jia et al. [16] investigated the friction coefficient and wear rate within a single rod and the surrounding interrod region. It has been reported that the wear depth and friction coefficient is larger in interrod region compared to the rod one [15]. Friction and wear resistance along the axis perpendicular to rods is observed to be slightly better than the one along the axis parallel to

rods. Even though the anisotropic friction and wear properties of enamel were investigated through experimental approaches, as far as the author's knowledge, few numerical simulations focus on the effective wear of enamel with consideration of the microstructure of enamel and the local mechanical properties and wear characteristics of its rod and interrod phases. The optimal orientations obtained can be inspiring for designing artificial wear-resistance composites.

The present work aims at numerically studying how the local wear properties of enamel and the geometric features of its enamel microstructure relate to its macroscopic wear while applying some newly introduced concepts of the micromechanics of wear [17]. A three-dimensional model of enamel is built up, accounting for the material properties and microstructure of rods and interrods in enamel. The key-hole shaped cross-section of rods and the angle between long-axis of rods and sliding direction of counterpart in contact are taken into consideration, as illustrated in Fig. 1. The corresponding frictional unilateral contact problem with wear is solved by the finite-element (FE) method. Assuming that the local wear of rod and interrod phases follows Archard's law. The wear coefficients of vertical and oblique rods are compared under different sliding directions. The results obtained suggest that an optimal fibrous structure exists. The lowest wear among enamels with different rod orientations is related to the microstructure, bulk material properties (elastic modulus, Poisson's ratios), frictional coefficients and and wear coefficients of the rod and interrod phases in enamel.

The rest of the paper is organized as follows. In Section 2, elements of a recently proposed micromechanics theory of wear are recalled for the purpose of the present work, and the three-dimensional finite element model for the unilateral contact of enamel and food with wear is presented. Section 3 is dedicated first to determinining a representative surface element (RSE). In Section 4, main numerical results are given and discussed. Some concluding remarks are provided in section 5.

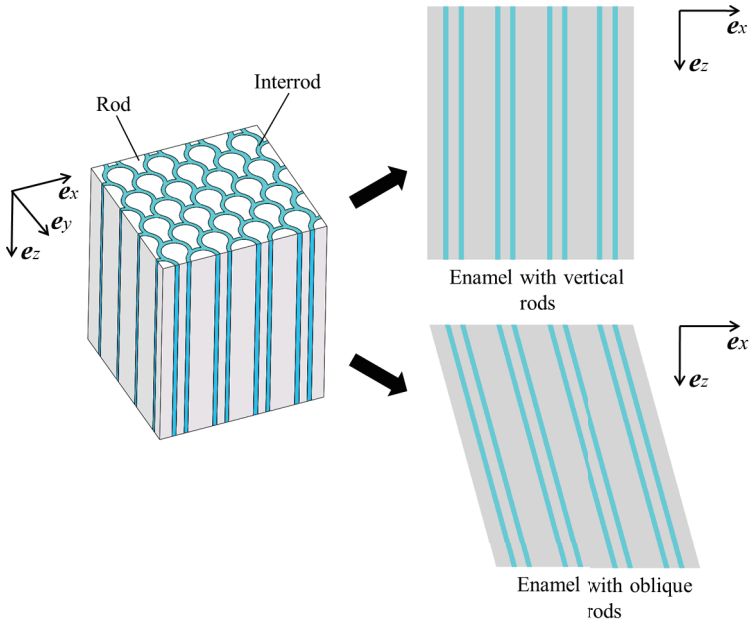

Figure 1: Three-dimensional model of enamel with vertical or oblique key-hole shaped rods

2. Wear model of enamel

2.1. Wear of enamel as a two-phase composite

Enamel is a complex biocomposite whose structure is hierarchical. In the present work, only two scales are considered, i.e. the microscopic and macroscopic ones are considered. By the microscopic scale, we mean a few micrometers where the mechanical properties of the rod and interrod phases can be experimentally identified by nanoindentation or nanoscratch [18, 19]. At this scale, enamel can be considered as a two-phase periodic composite. Precisely, it is made of an rod phase coated with an interrod phase. In determining the effective bulk properties of enamel, a unit cell of its microstructure acts as a *representative volume element* (RVE) in the sense of micromechanics (see, e.g., [20, 21, 22, 23]). However, in investigating the effective (or macroscopic) wear of enamel, a *representative surface element* (RSE) S as the surface counterpart of RVE may need containing the surfaces of several unit cells of its bulk microstructure. This important issue of determining a RSE for enamel will be studied in detail in the next section.

In what follows, the rod and interrod phases of enamel are referred to as phases 1 and 2,

respectively. Let S_i be the subdomain of a RSE S of enamel occupied by phase i $(= 1, 2)$. The area fractions of these two constituent phases are defined by

$$f_i = \frac{|S_i|}{|S|} \tag{1}$$

where $|S_i|$ and $|S|$ represent the areas of S_i and S, respectively. Clearly, we have $f_1 + f_2 = 1$. The normal force P sustained by the RSE S of enamel consists of two parts:

$$P = P_1 + P_2. \tag{2}$$

where P_1 and P_2 are the normal forces applied to the subdomains S_1 and S_2 of S.

In the present work, the isotropic Achard wear law [24] is adopted to describe the local wear of the rod and interrod phases of enamel. Consequently, the volumetric wear rate $\dot{W}_i$ of phase i is given by

$$\dot{W}_i = \frac{K_i}{H_i} P_i v \tag{3}$$

where H_i and K_i are the respective hardness and wear coefficient of phase i, P_i is the normal contact force supported by phase i and v the relative sliding speed which equals the norm $\|v\|$ of the relative sliding velocity v. As argued in Ref. [25], it is convenient to introduce the *normalized wear coefficient*

$$\hat{\eta}_i = \frac{K_i}{H_i} \tag{4}$$

and to rewrite (3) in the equivalent form

$$\dot{W}_i = \hat{\eta}_i P_i v. \tag{5}$$

The total wear rate of the RSE S in question is provided by

$$\dot{W} = \dot{W}_1 + \dot{W}_2. \tag{6}$$

Accounting for (5) in (6), we obtain

$$\dot{W} = (\hat{\eta}_1 P_1 + \hat{\eta}_2 P_2) v. \tag{7}$$

Further, under the condition that the normal contact force P_i supported by phase i is proportional to the total contact force P of the RSE S, i.e.

$$P_i = \zeta_i P \tag{8}$$

where the scalar $\zeta_i \in [0, 1]$ is the ratio of P_i to P, then the effective wear law follows from introducing (8) into (7):

$$\dot{W} = \eta^* P v. \tag{9}$$

In this formula, η^* represents the effective (normalized) wear coefficient of enamel and is given by

$$\eta^* = \zeta_1 \hat{\eta}_1 + \zeta_2 \hat{\eta}_2. \tag{10}$$

Noting that $P = P_1 + P_2 = (\zeta_1 + \zeta_2)P$ so that

$$\zeta_1 + \zeta_2 = 1, \tag{11}$$

then equation (10) can further be written as

$$\eta^* = \hat{\eta}_1 + \zeta_2(\hat{\eta}_2 - \hat{\eta}_1) = \hat{\eta}_2 + \zeta_1(\hat{\eta}_1 - \hat{\eta}_2). \tag{12}$$

This formula implies that it suffices to compute either of ζ_1 and ζ_2 for determining η^* if $\hat{\eta}_1$ and $\hat{\eta}_2$ are given.

2.2. FE contact model and wear computation

The frictional contact between enamel and food or other hard objects is simulated by a three-dimensional (3D) FE model. At the microscopic scale, enamel can be assimilated to an assemblage of composite cylinders (Fig. 2) [4, 5]. Each composite cylinder consists of a rod coated by an interrod of thin thickness, and its cross-section is of key-hole shape. The composite cylinders of enamel are periodically arrayed in the cross-section plane. In this work, the area or volume fraction of the rods is taken to be 78% while that of the interrods is equal to 22%; in addition, the largest head size of the rods in enamel is set to $5\mu m$. As a first approximation, the food or other objects in food is represented by a ball whose radius is of $500\mu m$. Denoting by ϕ the inclination angle between the long-axis of the rods of enamel and

the direction $\mathbf{e}_z$ along which contact pressure will be applied, three values will be considered for ϕ, i.e. $\phi = 5°$, $15°$ and $30°$ (see Fig. 2).

The unilateral contact between the upper ball and the enamel surface initiates at the center of a rod and spreads over a surface domain whose size is required to be not smaller than a RSE. Then, the frictional sliding of the upper ball on the enamel surface consists of a forward movement along the direction $-\mathbf{e}_x$ and a backward one along the opposite direction $\mathbf{e}_x$. The total sliding distance accomplished during such a cycle is denoted by L.

The appropriate normal displacement (or contact force) has to be imposed so that the contact surface covers a RSE of enamel. The normal displacement used is $0.3\mu m$, generating a circular contact area whose radius is of about $20\mu m$, as detailed in Section 3. Thus, the contact region covers around 15 rods of enamel. A minimum sliding distance is required to ensure that the contact status of two surfaces be in total slip without stick. Two values for the frictional coefficient μ are adopted, namely $\mu = 0.1$ and 0.3.

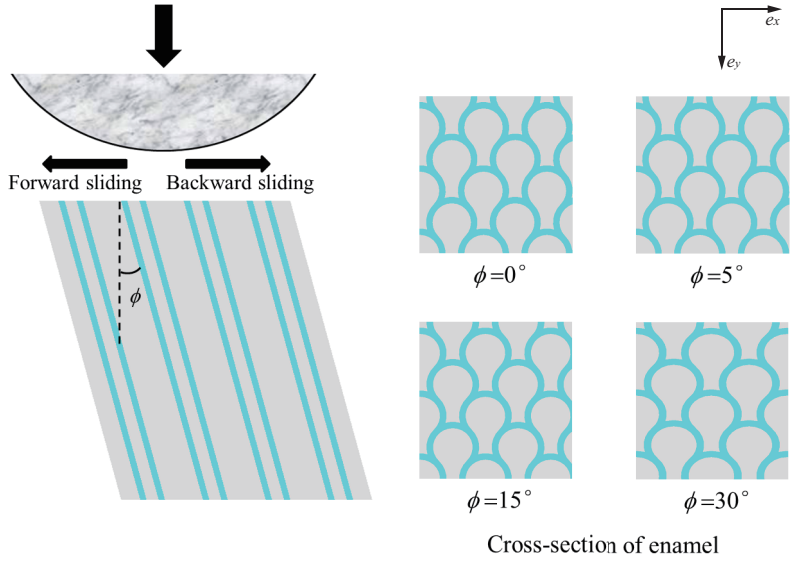

Figure 2: The different inclination angles of rods in enamel: ϕ =0°, 5°, 15° and 30°. The sliding movements of a ball in $-\mathbf{e}_x$ and $\mathbf{e}_x$ are, respectively, referred to as "Forward" and "Backward".

One complete cycle is composed of J substeps and there are N nodes in the contact region belonging to rod or interrod phase. The letters j and n represent the current substep and a node of i-th phase ($i = 1$ and 2 for the respective rod and interrod phases), respectively.

The nodal frictional stress τ^j and relative sliding distance δ^j are determined by the contact condition of the j-th substep. The wear loss at n-th node is evaluated based on the discretized Archard's wear law and recorded as temporary data, as follows

$$\Delta h^j = \eta_i p^j (\delta^j - \delta^{j-1}), \tag{13}$$

where η_i and represents the *nodal wear coefficient* of the rod or interrod phase. The term $(\delta^j - \delta^{j-1})$ is the relative sliding distance at current step. Equation (13) amounts to discretizing the material volumetric wear into a nodal depth variation [26] and [27]. Notice that, in total sliding condition, the nodal frictional (or shear) stress τ^j is proportional to the nodal contact pressure p^j according to the Coulomb's frictional law, namely $\tau^j = \mu p^j$ with μ being the friction coefficient. The substeps should be small enough so that the variation of p^j during the sliding cycle of the ball head is negligible. The variation Δh of the depth of node n in one cycle is the accumulation of those in all substeps:

$$\Delta h = \eta_i \sum_{j=1}^{J} p^j (\delta^j - \delta^{j-1}). \tag{14}$$

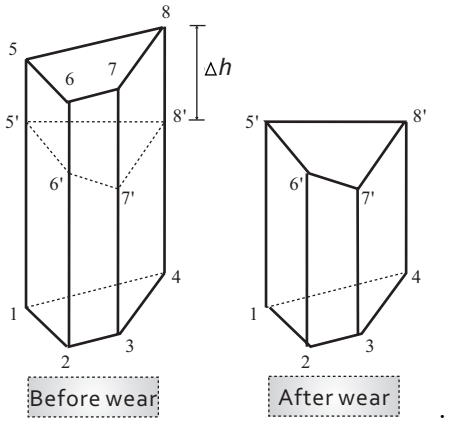

Figure 3: Computation of the wear volume of one element SOLIDE185 in the FE model

The element type adopted for enamel is the solid element "SOLIDE185" in the software ANSYS which is hexahedron; and the total amount of elements is 955280. The volumetric wear is calculated according to the coordinates variations of the 4 nodes on the contact

surface of such an element, i.e. the volume of the body $\Omega_{5678-5'6'7'8'}$ in Fig. 3. The nodal wear depths can be correspondingly converted to the rod and interrod wear volumes, W_1 and W_2,. The normal loads P_1 and P_2 the rod and interrod phases bear during sliding can be obtained from contact analysis. Starting from (9), we calculate the apparent (normalized) coefficients $\hat{\eta}_i$ of the constituents and the (normalized) effective wear coefficient η^* of the enamel as follows:

$$\hat{\eta}_i = \frac{W_i}{LP_i}, \qquad \eta^* = \frac{W_1 + W_2}{LP}, \tag{15}$$

where L is the sliding distance.

The values used for the material parameters of the rod and interrod phases are given below:

— Rod: $E_1 = 90$ GPa, $\nu_1 = 0.3$, $\eta_1 = 2 \times 10^{-6}$;

— Interrod: $E_2 = 39.5$ GPa, $\nu_2 = 0.35$, $\eta_2 = 2 \times 10^{-5}$;

— Ball: $E_b = 82$ GPa, $\nu_b = 0.25$.

Note that, among the numerical values listed above and used in the present work, those of E_1 and E_2 correspond to the ones obtained experimentally [10, 28, 29]; those of E_b and ν_b are the ones of rock reported in Ref. [30]; those of ν_1, ν_2, η_1 and η_2 are hypothetical, since no experimentally determined values seem to be available for them. The boundary conditions of the model(see Fig. 4) are as follows:

— On the lower cross-section surface S^{lower} of Ω,

$$u_x = u_y = u_z = 0$$

— On the lateral surface T^2 and T^4 of Ω,

$$u_y = 0, t_x = t_z = 0,$$

— On the lateral surface T^3 of Ω,

$$u_x = 0, t_y = t_z = 0,$$

— On the lateral surface T^1 of Ω,

$$u_x = 0, t_y = t_z = 0, \text{during the normal loading}$$

$$u_x = \bar{u}, t_y = t_z = 0, \text{during the sliding}$$

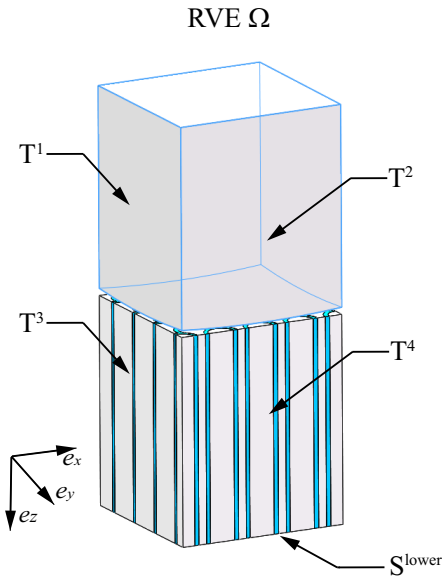

Figure 4: The boundary conditions of the model

3. Determination of a RSE

A *representative surface element* (RSE) of enamel used in finite element analysis has to be sufficiently large so that the wear computation results are independent of the rods and interrods involved. It is important to note that, even though the microstructure of enamel is periodic in the cross-section plane, a RSE cannot be taken to be just a unit cell of this microstructure. Indeed, since the wear computation is carried out through a ball of radius r indented on and sliding over the surface of enamel, the resulting circular contact domain of radius a must be large enough so that the effective wear per unit area is independent of the number of rods and interrods involved in the contact region.

The ball indenting enamel slides along three directions: the $\mathbf{e}_x$-direction, the $\mathbf{e}_y$-direction and the direction of 45° (Fig. 5). The numerical results obtained are provided there. These results show: (i) once the radius a of the contact domain is approximatively 5 times larger than the rod head size r, i.e. $a/r \gtrsim 5$, corresponding to a normal displacement of $0.3mm$ for the material parameter values used, the effective wear per unit area is almost constant;

(ii) the effective wear amounts along the three directions in question present a difference lower than 5%. The result (i) means that, when $a/r \gtrsim 5$, the contact surface in question can be considered as an RSE. The result (ii) implies that the macroscopic wear is almost isotropic, even the microstructure is not isotropic. The last conclusion is not surprising due to the Neumann principle [31]: the symmetry group of a macroscopic property of a material includes the one of its microstructure as a subgroup.

In conclusion, concerning the wear computation in question, the radius of the contact region must be at least 5 times larger than the head size of a rod in enamel. Thus, when this sufficient condition is satisfied, the contact surface can be considered as a RSE for the wear simulation of enamel.

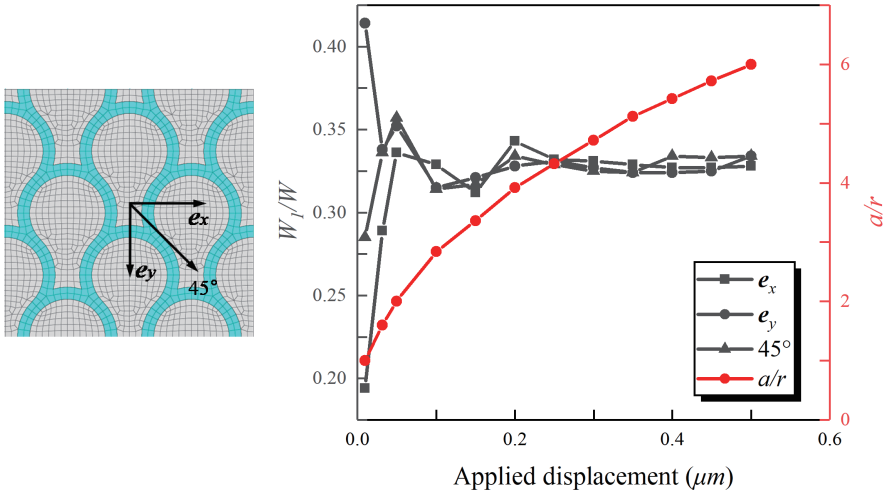

Figure 5: Representative Surface Element (RSE) of enamel - the minimum contact surface of which the effective (normalized) wear coefficient η^* of enamel is independent on neither sliding direction nor sliding distance

4. Results and discussion

4.1. Wear of enamel with vertical and oblique rods

In this section, by the finite element method and in light of the micromechanics concepts introduced in Section 2, we numerically determine the (normalized) effective wear coefficient η^* of enamel through using (15) and discuss the influences of key factors on η^*. Three factors

are considered. First, the rods in enamel are taken to be vertical and oblique; precisely, the inclination angle ϕ is equal to 0°, 5°, 15° and 30°. Second, two values, i.e. 0.1 and 0.3, are employed for the friction coefficient μ. Third, the direction of sliding the ball on the enamel surface is distinguished according as it is forward or backward with respect to the inclination of rods in enamel.

Concerning the rod phase, when the inclination angle ϕ increases from 0° to 30°, the apparent wear coefficient $\hat{\eta}_1$ augments monotonously in both the cases of $\mu = 0.1$ and $\mu = 0.3$ and in both the forward and backward sliding (Fig. 6(a) and Fi.g. 7 (a)). This augmentation appears more important during the forward sliding. Note also that the difference between the values of the apparent wear coefficient associated to the forward and backward sliding gets larger while the friction coefficient increases.

In regard to the interrod phase, when the inclination angle ϕ varies from 0° to 30°, the tendency is inverse. More precisely, the apparent wear coefficient $\hat{\eta}_2$ decreases with the increase of ϕ for $\mu = 0.1$ and $\mu = 0.3$ and for the forward and backward sliding (Fig. 6(b) and Fi.g. 7 (b)). This decreases becomes more pronounced when the forward sliding is in question. Remark again that the difference of the values of the apparent wear coefficient relative to the forward and backward sliding becomes more important when the friction coefficient increases.

The wear amount of enamel is the sum of those of the rod and interrod phases. The numerical results show that, when the inclination angle ϕ of the rod phase takes 0°, 5°, 15° and 30°, the effective (nomalized) wear coefficient η^* of enamel is maximum when $\phi = 15°$ regardless of the two friction coefficient values used, i.e. $\mu = 0.1$ and $\mu = 0.3$ (Fig. 6). This holds for both the forward and backward sliding cases (Figs. 6 and 7). The numerical results also show that, when the forward sliding is concerned, the minimum value of the effective (nomalized) wear coefficient η^* of enamel occurs when $\phi = 0°$. However, when the backward sliding is in question, the minimal value of η^* of enamel appears when $\phi = 30°$ (Fig. 6).

To explain the numerical results given above, recall equation (12). According to this formula, the ratio ζ_1 of the normal force P_1 supported by the rod phase to the total normal force P applied is the key to determining the effective wear coefficient η^* of enamel. The

elastic modulus of the rod phase is 2.27 times larger than the one of the interrod phase and and 10 times more wear-resistant than the interrod phase. The more load that the rods undertakes, the less load is left for the matrix phase and the effective wear of enamel is reduced. The lowest value of the load ratio ζ_1 of the rod phase in Fig. 8 (a) and (b) corresponds to the largest value of the effective wear coefficient of enamel (Fig. 6(c) and 7(c)).

4.2. Optimal effective wear coefficient of enamel

Apart from the effect of load ratio ζ_1, the effective wear coefficient η^* of enamel is also affected by the wear coefficients of the rod and interrod phases. The microscopic wear volume can be identified experimentally by nanoscratch tests and it is found that the wear of interrod phase is larger than that of rod phase i.e., $\hat{\eta}_1 < \hat{\eta}_2$, $\eta_1 < \eta_2$ [13, 19]. However, the wear measured by nanoscratch could be affected by sample preparation and indentation parameters, which result in a large deviation of the value of $\hat{\eta}_1$, $\hat{\eta}_2$, η_1 and η_2. In the numerical application, we adopt a wide range of wear coefficients at FE nodes, in order to investigate the effect of the ratio η_2/η_1 on the maximum and minimum values of the effective wear coefficient η^* while considering different inclinations of the rod phase.

In Fig. (9-12), η^* is linearly related to η_2/η_1 and the slopes of ϕ in the different cases are slightly different. In order to better illustrate the intersection points of the four lines, the enlarged images are attached below. We mainly focus on the maximum and minimum values of η^* in different ranges of η_2/η_1. In the case of forward sliding with $\mu = 0.1$, the maximum η^* occurs, as in Fig. (9), at: $\phi = 30°$ when $\eta_2/\eta_1 \in [1, 9.02]$; $\phi = 15°$ when $\eta_2/\eta_1 \in [9.02, 11.91]$; $\phi = 5°$ when $\eta_2/\eta_1 \in [11.91, 26.49]$; $\phi° = 0$ when $\eta_2/\eta_1 \in [26.49, +\infty]$. In the case of backward sliding, the maximum η^* takes place at $\phi = 30°$, 15°and 5° according as η_2/η_1 belongs to [1, 7.82], [7.82, 12.92], [12.92, $+\infty$] as shown in Fig. (10) and Fig. 13(a). When $\mu = 0.3$ of forward sliding, the intersection points of the four lines change slightly and the maximum value is observed at $\phi = 30°$, 15°, 5° and 0° with η_2/η_1 belonging to [1, 9.16], [9.16, 11.2], [11.2, 17.24], [17.24, $+\infty$], respectively, as shown in Fig. (11) and Fig. 13(a).

The minimum of the effective wear of enamel is observed to appear only when $\phi = 0°$

or 30°. In the case of forward sliding with $\mu = 0.1$, the minimum value of η^* is achieved at $\phi = 0°$ when $\eta_2/\eta_1 \in [1,\ 10.86]$ and at $\phi = 30°$ when $\eta_2/\eta_1 \in [10.86,\ +\infty]$, as shown in Figs. (9) and Fig. (13(b)). In both the forward and backward sliding conditions, the minimum of the effective wear of enamel occurs for $\phi = 0°$ or $\phi = 30°$ according as η_2/η_1 is smaller or larger than a critical value Fig. (13(b)).

In our model with numerical applications, the best wear resistance is the enamel with vertical rods provided η_2/η_1 varies within a certain range. This range is dependent on the relative sliding direction and friction coefficient (Fig. 13b). As an extension, for a fiber-reinforced composite, the optimal orientation of fibers with the best wear resistance is associated with the friction coefficient, volume fraction and the elastic parameters of fibers and matrix which corresponds to the rod and interrod phases for tooth enamel. From the optimal orientation of the rods of enamel we can learn how the microstructure of fibrous composites affects its macroscopic wear. The optimal orientations obtained are not necessarily found in the teeth of people or other animals but can be inspiring for designing artificial wear-resistance composites.

4.3. Efficiency of breaking food

The main function of teeth is the smashing and grinding food between upper and lower teeth into small pieces. In our model, the food is assimilated as the upper ball in contact with enamel. The failure property of food is assumed to be characterized by von-Mises stress, giving rise to the distribution shown in Fig. 14. In fact, one of the main difficulties in simulating the fragment of food is due to the large variety of foods in terms of their physical/mechanical behaviors and geometrical shapes, which may be met in such a process. Assimilating food to an elastic ball may appear to be oversimplified but this is a first step toward constructing more realistic model. However, even with our first-step model, the food breaking process can be simulated in an approximate way and the useful first-order results about it can be obtained in some cases such as in investigation of the teeth of rodent animals.

The efficiency of enamel is here evaluated by the maximum value of the von-Mises stress of the ball (assimilated to food) divided by the normal load. The enamel with oblique rods

has higher efficiency compared with the one with vertical rods, and the enamel with rods of $\phi = 30°$ exhibits the highest efficiency for a given friction coefficient value and along a given sliding direction. The larger friction coefficient results in greater shear stress at local area and is more efficient in breaking food. With the same friction coefficient, the forward sliding movement appears always more effective in comparison to the backward sliding, as shown in Fig. (15).

5. Closing Remarks

To sum up, the present work numerically studies how the local wear properties of enamel and the geometric features of its microstructure relate to its macroscopic wear while applying some newly introduced concepts of the micromechanics of wear [17, 20, 25]. The key-hole shaped rod and interrod phases are builded up by three dimensional finite element model while considering different inclinations of rods. The wear volumes of rod, interrod phase and enamel are discretized as the variations of nodal depths, which are related to the nodal wear coefficient, local contact pressure and relative sliding distance. To be a RSE, the contact region should cover at least 15 rods. The effects of the friction coefficient, sliding directions, wear coefficients of the rod and interrod phases, and the inclination angle of rods on the effective (normalized) wear coefficient are numerically analyzed. A simplified evaluation of efficiency of different inclined rods in grinding food or hard objects is carried out in this study.

The methodology we propose necessitates identifying the wear coefficients of the rod and interrod phases of enamel. Now, these microscopic properties can be identified experimentally by nanoindentation or nanoscratch tests [10, 18, 19]. However, a micromechanical model allows estimating the effective wear coefficient of enamel in terms of its microscopic phases and microstructure, and this model is of theoretical and practical interest at least for two reasons. First, it helps us in getting a better understanding of the biomechanical behavior of enamel; Second, it is useful and inspiring for designing and fabricating the relevant biomimetic materials.

The following remarks can be drawn from this work:

(I) The effective wear coefficient of enamel depends on the relative sliding direction and the friction coefficient. Four values, namely 0°, 5°, 15° and 30°, have been considered for the inclination angle ϕ of the rod phase. The effective (nomalized) wear coefficient η^* of enamel turns out to be maximum when $\phi = 15°$ regardless of the two friction coefficient values used. The minimum value of η^* of enamel occurs at $\phi = 0°$ or 30° according to the sliding direction is forward or backward.

(II) An optimal wear resistance of the enamel exists and depends on the sliding direction and the local tribological properties of the rod and interrod phases. The minimum wear of enamel appears at $\phi = 0°$ and $\phi = 30°$ when η_2/η_1 is, respectively, smaller and larger than a critical value. As an extension, for a fiber-reinforced composite, the optimal inclination angles of fibers with best wear resistance is associated with the friction coefficients, volume fraction and the elastic parameters of fibers and matrix. The numerical model can be helpful in selecting the angle of fibers to meet the requirement of the specified wear property of the composite.

(III) The forward sliding movement, a significant inclination angle of rods and a large friction coefficient are factors favorable to the high efficiency of breaking food.

Acknowledgements

We acknowledge the financial support provided by the National Natural Science Research Foundation of China No. 11572266, China Postdoctoral Science Foundation No. 2018M633362.

References

[1] Z.R. Zhou, H.Y. Yu, J. Zheng, L.M. Qian, Y. Yan, Dental Biotribology. Springer, Berlin, 2013.

[2] B. Bar-on, H.D. Wagner. Enamel and dentin as multi-scale bio-composites. Journal of the Mechanical Behavior of Biomedical Materials 12 (2012) 174-183.

[3] Ang, S.F., Bortel, E.L., Swain, M.V., Klocke, A., Schneider, G.A. Size-dependent elastic/inelastic behavior of enamel over millimeter and nanometer length scales. Biomaterials 31 (2010) 1955-1963.

[4] C. Lu, T. Nakamura, C.S. Korach, Effective property of tooth enamel: Monoclinic behavior, Journal of Biomechanics 45 (2012) 1437-1443.

[5] Y.J. Yoon, I.-H. Kim, S.-Y. Han, The reason why a sheath exists in enamel, International Journal of Precision Engineering and Manufacturing 16 (2015) 807-811.

[6] F.Z. Cui, J. Ge, New observations of the hierarchical structure of human enamel, from nanoscale to microscale, Journal of Tissue Engineering and Regenerative Medicine 1 (2007) 185-191.

[7] P.S. Ungar, L.H. Claire, N.W. Alexa, T.F. Mark, Dental topography and microwear texture in Sapajus apella. Biosurface and Biotribology (2018) 124-134.

[8] Z.Y. Weng, Z.Q Liu, R.O. Ritchie, D. Jiao, D.S. Li, H.L. Wu, L.H. Deng, Z.F. Zhang, Giant panda's tooth enamel: Structure, mechanical behavior and toughening mechanisms under indentation, Journal of the Mechanical Behavior of Biomedical Materials 64 (2016) 125-138.

[9] H. Xiao,L. Lei, J.P. Peng, D. Yang, Q.H. Zeng, J. Zheng, Z.R. Zhou, Research of the role of microstructure in the wear mechanism of canine and bovine enamel, Journal of the Mechanical Behavior of Biomedical Materials, 92 (2019) 33-39.

[10] J. Ge, F.Z. Cui, X.M. Wang, H.L. Feng, Property variations in the prism and the organic sheath within enamel by nanoindentation, Biomaterials 26 (2005) 3333-3339.

[11] S.F. Ang, M. Saadatmand, M.V. Swain, A. Klocke, G.A. Schneider, Comparison of mechanical behaviors of enamel rod and interrod regions in enamel, Journal of Materials Research 27 (2012) 448-456.

[12] L.H. He, M.V. Swain, Nanoindentation creep behavior of human enamel, Journal of Biomedical Materials Research Part A 91 (2009) 352-359.

[13] J. Zheng, Y.Y. Zeng, J. Wen, L. Zheng, Z.R. Zhou, Impact wear behavior of human tooth enamel under simulated chewing conditions, Journal of the Mechanical Behavior of Biomedical Materials 62 (2016) 119-127.

[14] J. Zheng, Y Huang, L.M. Qian, Z.R. Zhou, Nanomechanical properties and microtribological behaviours of human tooth enamel, Proceeding of the Institution of Mechanical Engineers, Part J: Journal of Engineering Tribology 224 (2009) 577-587.

[15] Y.R. Jeng, T.T. Lin, M. Hsiu, H.J. Chang, D.B. Shieh, Human enamel rod presents anisotropic nanotribological properties, Journal of the Mechanical Behavior of Biomedical Materials 4 (2011) 515-522.

[16] Y.F Jia, F.Z. Xuan, Anisotropic wear behavior of human enamel at the rod level in terms of nanoscratching, Wear 290-291 (2012) 124-132.

[17] D. Yang, Q.C. He, Micromechanical estimation of the effective wear of elastoplastic fiber-reinforced composites, International Journal of Non-Linear Mechanics 108 (2019) 11-19.

[18] S. Habelitz, S.J. Marshall, G.W. Marshall Jr, M. Balooch, Mechanical Properties of human dentel enamel on the nanometer scale, Archives of Oral Biology 46 (2001) 173-183.

[19] S.Y. Zheng, J. Zheng, S.S. Gao, B.J. Yu, H.Y. Yu, L.M. Qian, Z.R. Zhou, Investigation on the microtribological behavior of human tooth enamel by nanoscrath, Wear 271 (2011) 2290-2296.

[20] S. Nemat-Nasser, M. Hori, Micromechanics: overall properties of heterogeneous materials, Elsevier Science Publishers, Amsterdam, 2013.

[21] Z. Hashin, Analysis of composite materials-a survey, Journal of Applied Mechanics 50 (1983) 481-505.

[22] G.W. Milton, The theory of composites, Cambridge University Press, Cambridge, 2002.

[23] S. Torquato, Reandom Heterogeneous Materials: Microstructure and Macroscopic Properties, Springer, New York, 2002.

[24] J.F. Archard, Contact and rubbing of flat surfaces, Journal of Applied Physics 24 (1953) 981-988.

[25] D. Yang, Q.C. He, A micromechanical approach to the wear of composites, submitted for publication, 2018.

[26] P. Podra, S. Andersson, Simulating sliding wear with finite element method, Tribology International, 32 (1999) 71-81.

[27] H. Benabdallah and D. Olender. Finite element simulation of the wear of polyoxymethylene in pin-on-disc configuration, Wear 261 (2006) 1213–1224.

[28] G. Willems, J.P. Celis, P. Lambrechts, M. Braem, G.Vanherle, Hardness and young's modulus determined by nanoindentation technique of filler particles of dental restorative materials compared with human enamel, Journal of Biomedical Materials Research 27 (1993) 747-755.

[29] M. Finke, J.A. Hughes, D.M. Parker, K.D. Jandt, Mechanical properties of in situ demineralised human enamel measured by AFM nanoindentation, Surface Science 491 (2001) 456-467.

[30] J. Thurn, R.F. Cook, Stress hysteresis during thermal cycling of plasma-enhanced chemical vapor deposited silicon oxide films, Journal of Applied Physics 91 (2002) 1988-1992.

[31] Q.S. Zheng, J.P. Boehler, The description,classification,and reality of material and physical symmetries, Acta Mechanica, 102 (1994) 73-78.

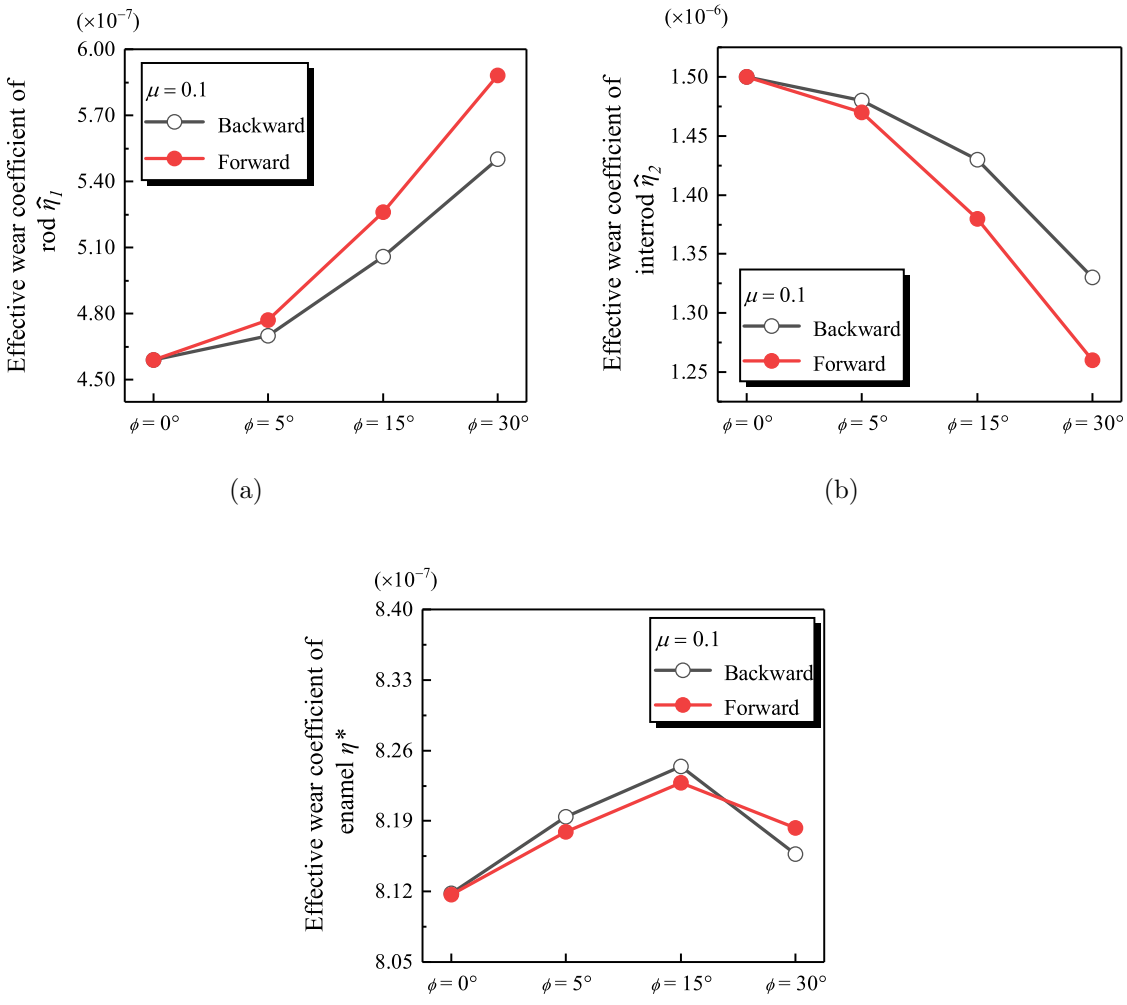

Figure 6: The apparent wear coefficients of the rod interrod phases, $\hat{\eta}_1$ and $\hat{\eta}_2$, and the effective wear coefficient η_* of enamel with vertical or oblique rods in the case of $\mu = 0.1$

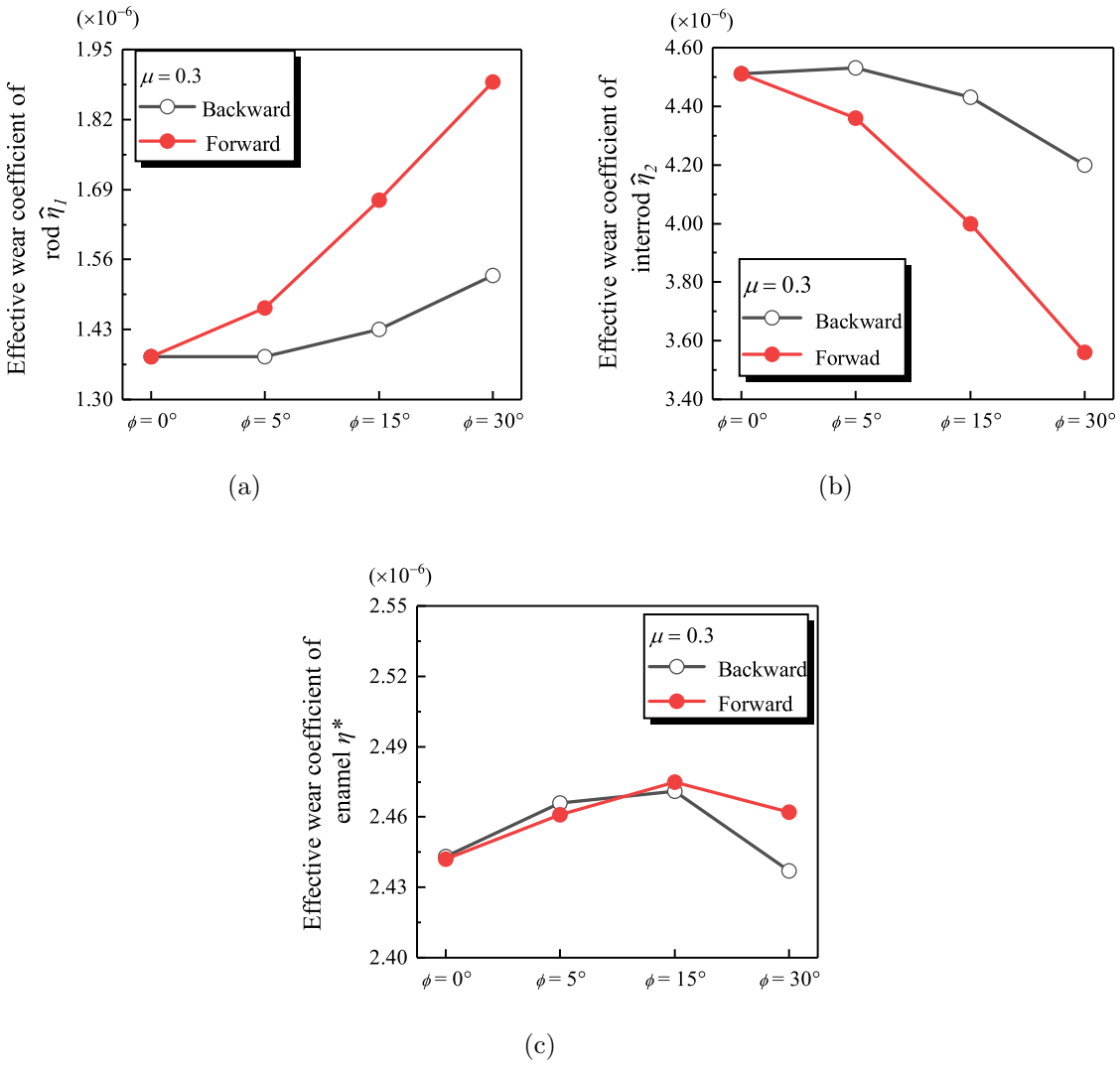

Figure 7: The apparent wear coefficient of the rod $\hat{\eta}_1$, interrod phase $\hat{\eta}_2$ and the effective wear coefficient η_* of enamel with vertical or oblique rods in the case of $\mu = 0.3$

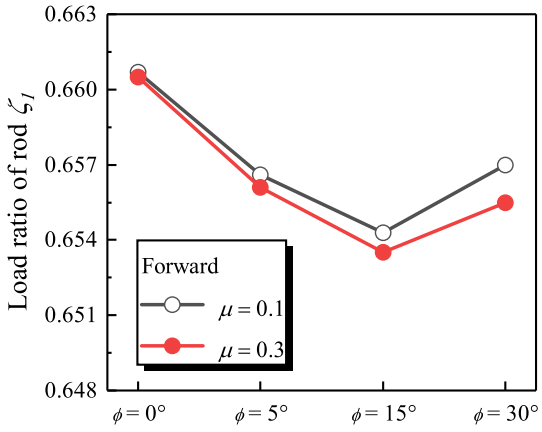

(a) ζ_1 in the case of forward sliding

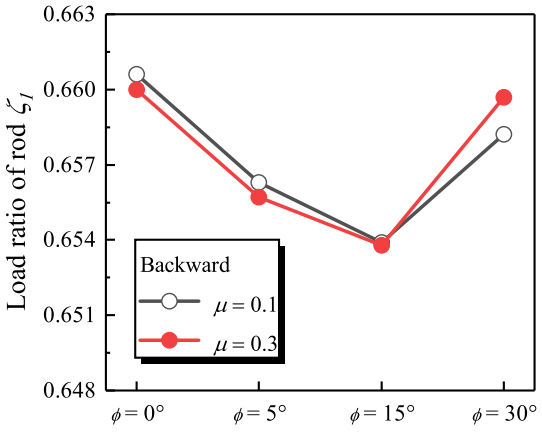

(b) ζ_1 in the case of backward sliding

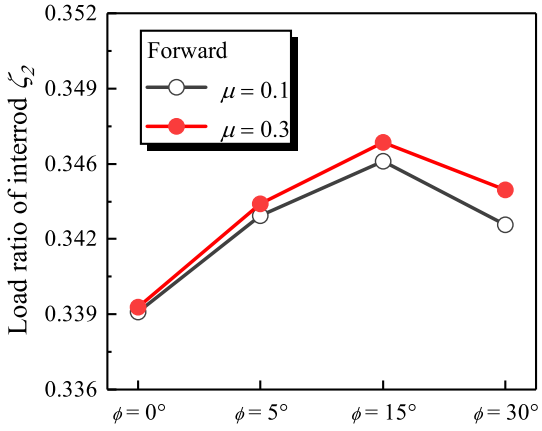

(c) ζ_2 in the case of forward sliding

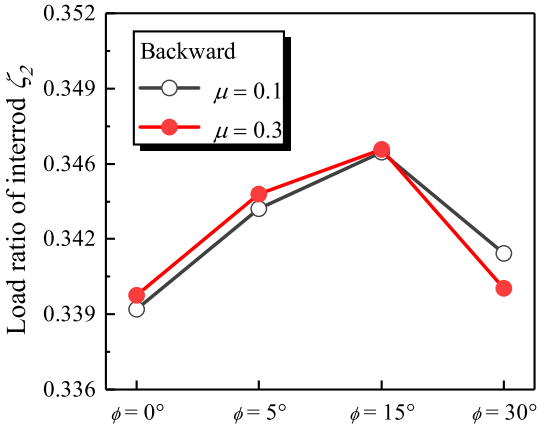

(d) ζ_2 in the case of forward sliding

Figure 8: The ratio ζ_1 of the load supported by the rod phase to that by the interrod phase during the friction and wear process and the ratio ζ_2 equal to $1 - \zeta_1$.

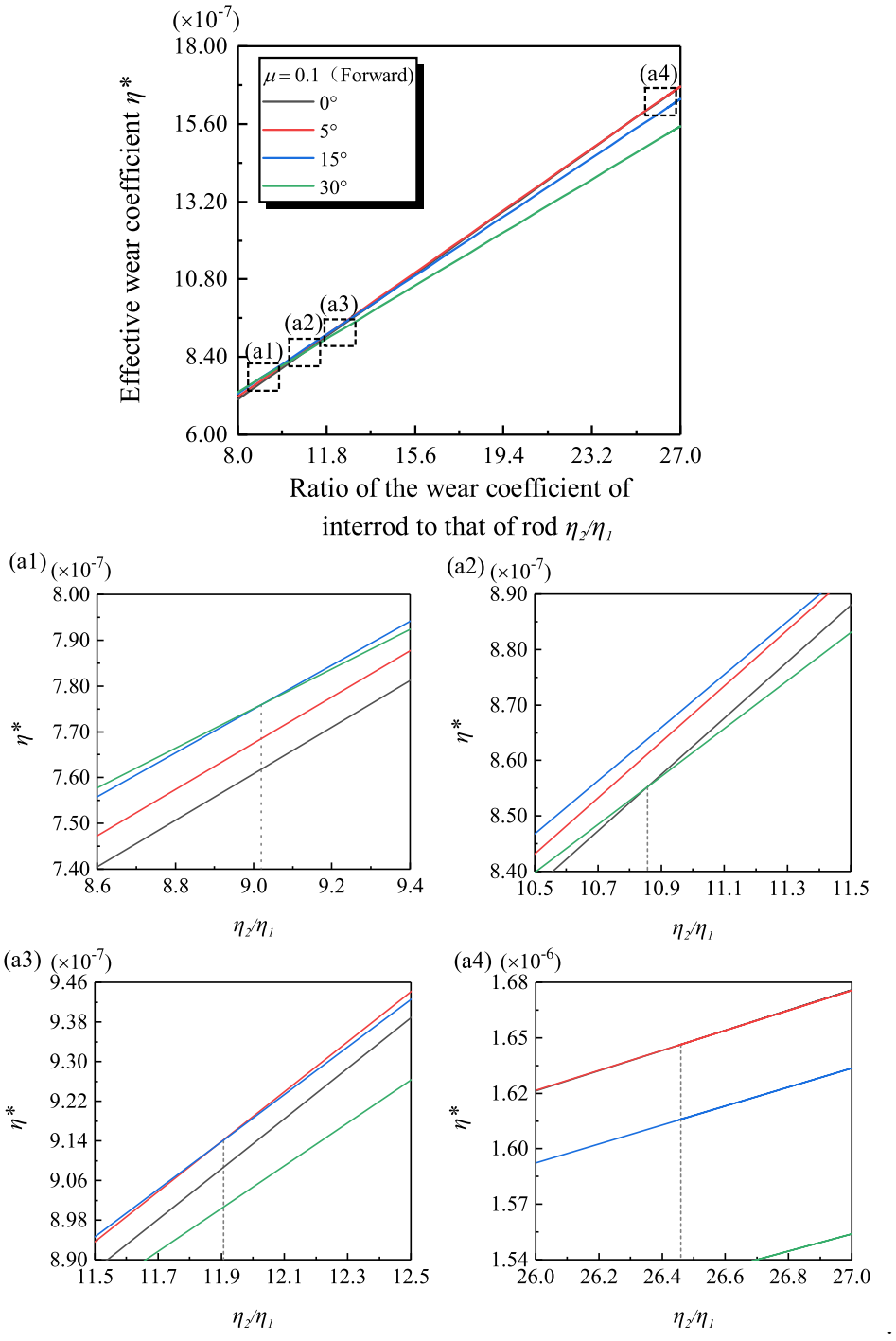

Figure 9: The effective wear coefficient η^* of enamel is linearly related to η_2/η_1. The inclination angle ϕ =0°, 5°, 15° and 30°. There are four lines and the neighborhood of intersection points are enlarged and shown in (a1)-(a4). The friction coefficient $\mu = 0.1$ and the sliding direction is forward.

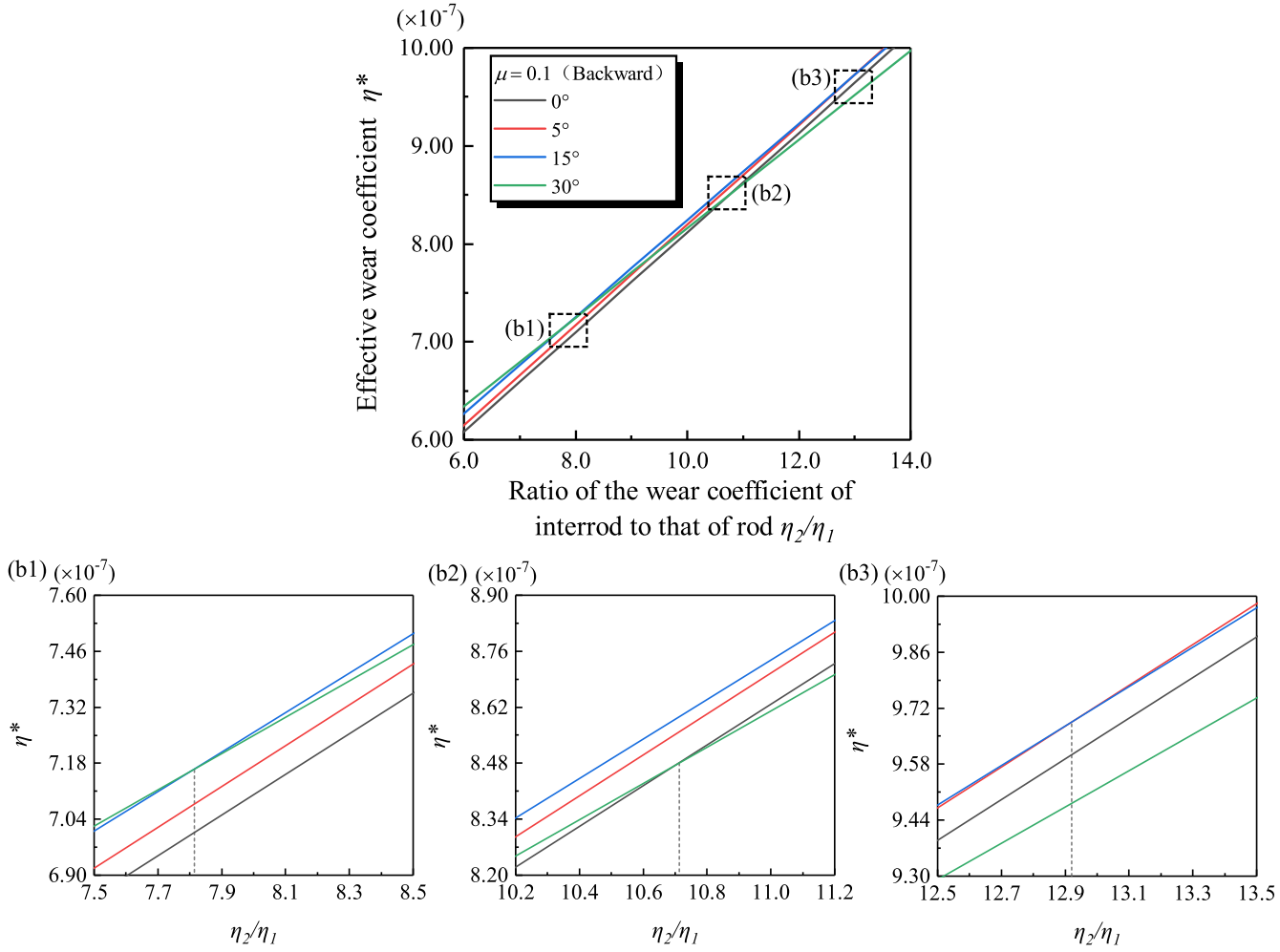

.

Figure 10: The effective wear coefficient η^* of enamel is linearly related to η_2/η_1. The inclination angle ϕ =0°, 5°, 15° and 30°. There are four lines and the neighborhood of intersection points are enlarged and shown in (b1)-(b3). The friction coefficient $\mu = 0.1$ and the sliding direction is backward.

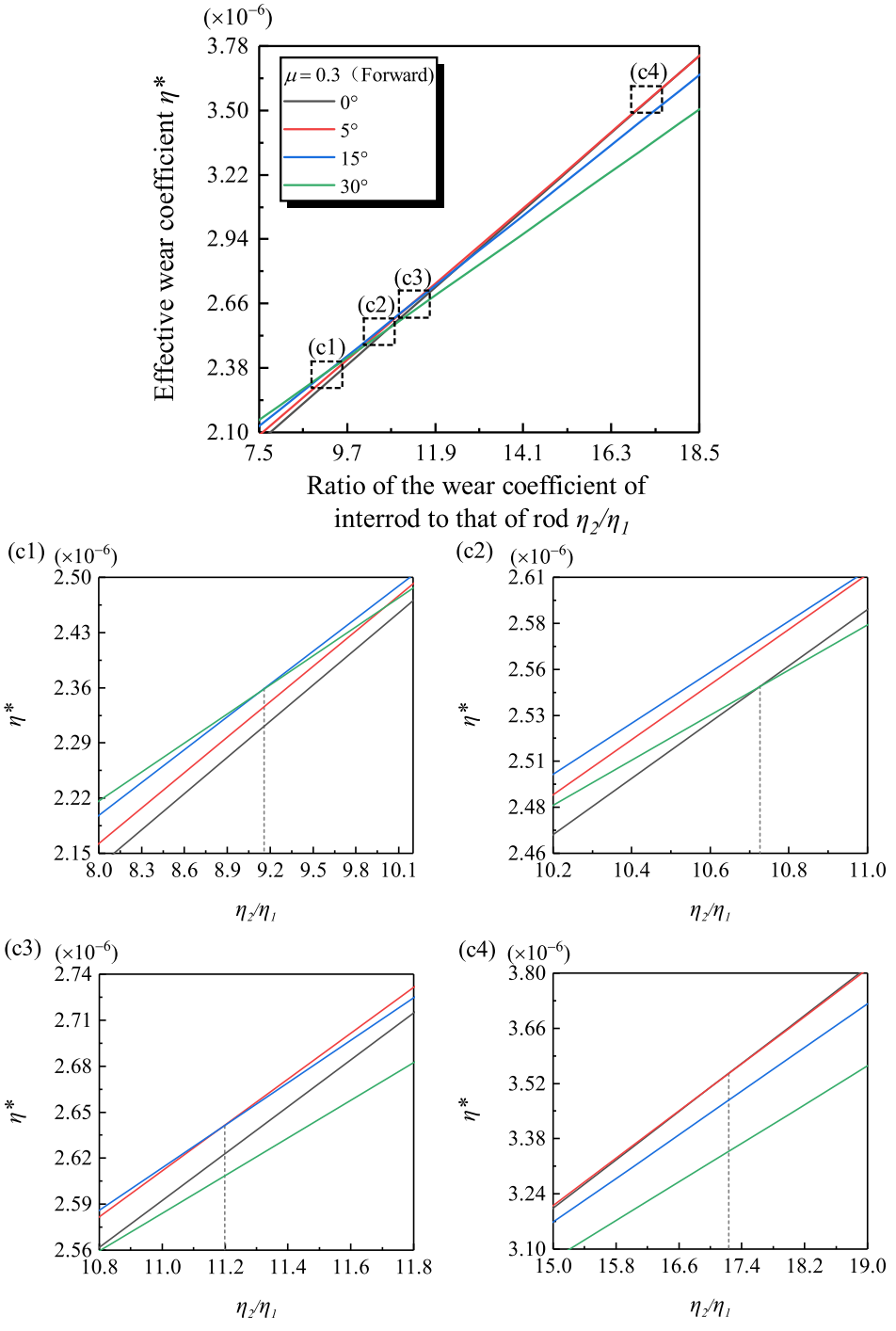

Figure 11: The effective wear coefficient η^* of enamel is linearly related to η_2/η_1. The inclination angle ϕ =0°, 5°, 15° and 30°. There are four lines and the neighborhood of intersection points are enlarged and shown in (c1)-(c4). The friction coefficient $\mu = 0.3$ and the sliding direction is forward.

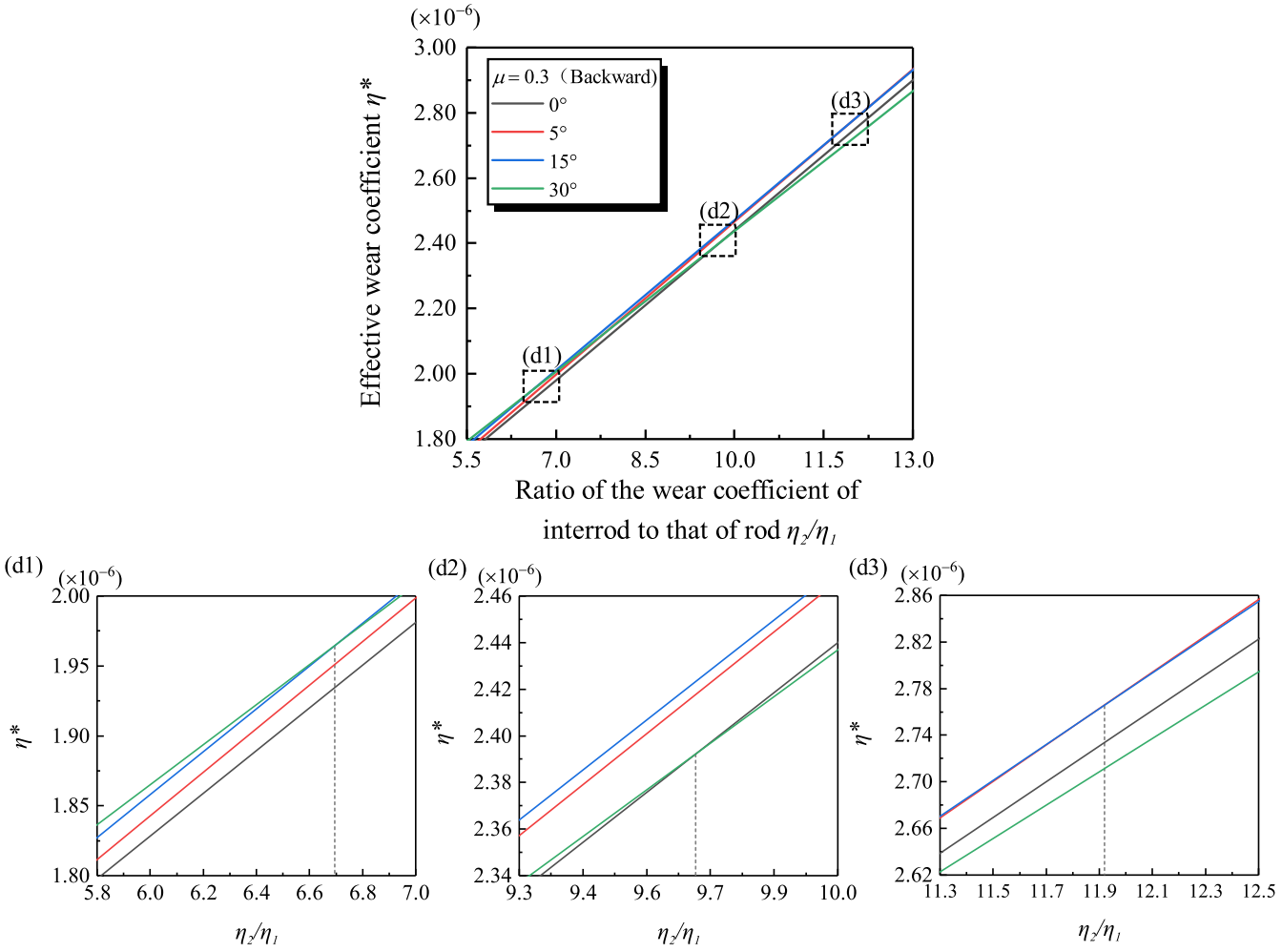

.

Figure 12: The effective wear coefficient η^* of enamel is linearly related to η_2/η_1. The inclination angle ϕ =0°, 5°, 15° and 30°. There are four lines and the neighborhood of intersection points are enlarged and shown in (d1)-(d3). The friction coefficient $\mu = 0.3$ and the sliding direction is backward.

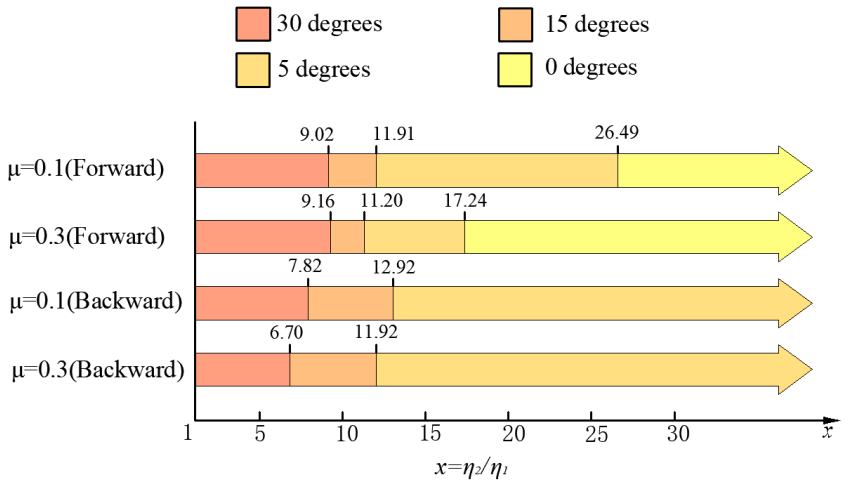

(a) The maximum value of η^* occurs at the enamel with rods of ϕ which is dependent on the value of η_2/η_1

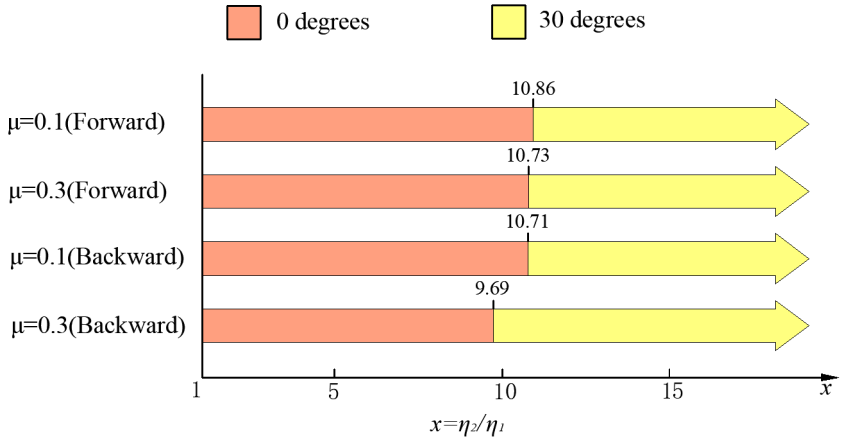

(b) The minimum value of η^* occurs at the enamel with rods of ϕ which is dependent on the value of η_2/η_1

Figure 13: The maximum and minimum values of the effective wear coefficient η^* of enamels are dependent on the ratio η_2/η_1 of the nodal wear coefficient of interrod to that of rods.

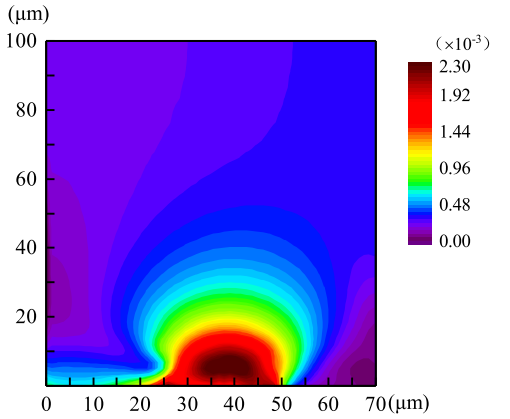

(a) Forward; Enamel with vertical rods $\phi = 0°$

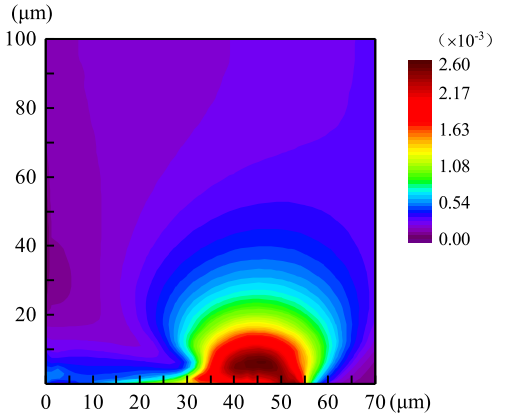

(b) Forward; Enamel with rods $\phi = 30°$

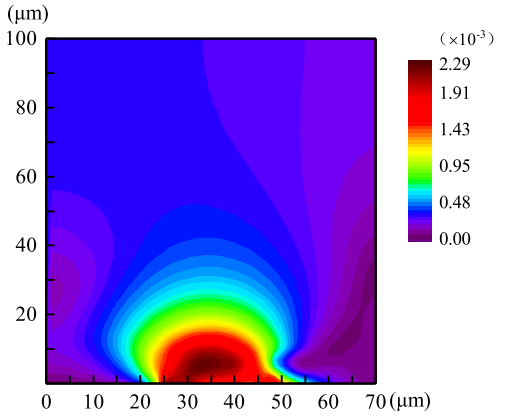

(c) Backward; Enamel with vertical rods $\phi = 0°$

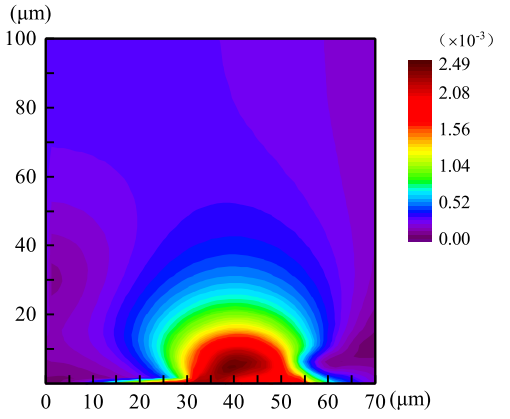

(d) Backward; Enamel with rods $\phi = 30°$

Figure 14: The distribution of normalized von-Mises stress of the ball when $\mu = 0.3$.

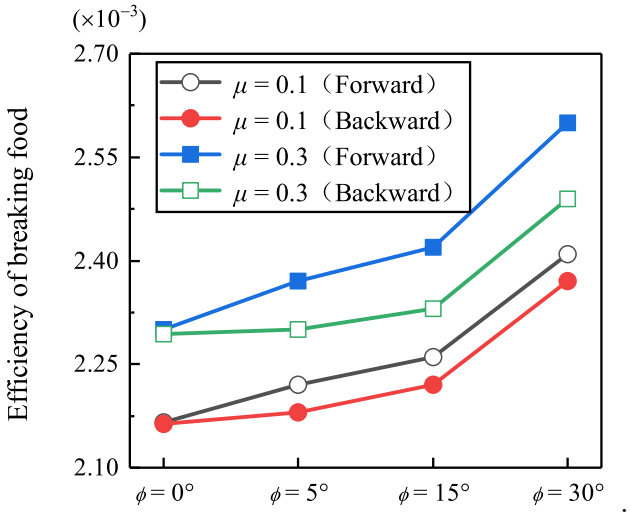

Figure 15: Efficiency of breaking food: the maximum value of the von-Mises stress of the ball (assimilated to food) divided by the normal load.